Corrections

MICROBIOLOGY

Correction for "Carbon and sulfur back flux during anaerobic microbial oxidation of methane and coupled sulfate reduction," by Thomas Holler, Gunter Wegener, Helge Niemann, Christian Deusner, Timothy G. Ferdelman, Antje Boetius, Benjamin Brunner, and Friedrich Widdel, which appeared in issue 52, December 27, 2011, of *Proc Natl Acad Sci USA* (108:E1484–E1490; first published December 12, 2011; 10.1073/pnas.1106032108).

The authors note that on page E1484, right column, first full paragraph, line 8, "the anaerobic oxidation of methane with sulfate (AOM) (**1**)" should instead appear as "the anaerobic oxidation of methane (AOM) with sulfate (**1**)."

Also on page E1484, right column, Eq. **2** and its explanation appeared incorrectly. The corrected equation and its corrected explanation appear below.

$$\Delta G^\circ = -16.6\ \text{kJ mol}^{-1}, \left(\frac{\{HCO_3^-\}\{HS^-\}}{\{CH_4(g)\}\{SO_4^{2-}\}}\right)_e = 10^{2.9} \quad [2]$$

(Index e indicates activity ratio applying for equilibrium, viz. $\Delta G = 0$; $\{H_2O\}$ is taken as 1) and thus one of the least exergonic processes sustaining life (ΔG in situ is often between −20 and −40 kJ mol^{-1}) (21–23).

On page E1485, right column, third full paragraph, lines 4–9, "If the subsequent reactions occur with reversibility and are viewed from the molecular perspective (that is, regarding microstates stochastically) at a given moment, the larger fraction of the enzyme molecules of each reaction performs the forward reaction, whereas a smaller fraction simultaneously performs the reverse reaction" should instead appear as "If subsequent reactions occur with reversibility and if the involved population of enzyme molecules is viewed from the molecular perspective (that is, regarding microstates stochastically) within a time interval in the range of an enzymatic turnover, the forward reaction is catalyzed more frequently than the reverse reaction."

On page E1487, right column, Eq. **11** within the footnote appeared incorrectly. The corrected equation appears below.

$$\left(\frac{\partial}{\partial T}\ln K_e\right)_p = \frac{\Delta H^\circ}{RT^2} \quad [11]$$

Last, Fig. 3 appeared incorrectly. The corrected figure and its corresponding legend appear below. These errors do not affect the conclusions of the article.

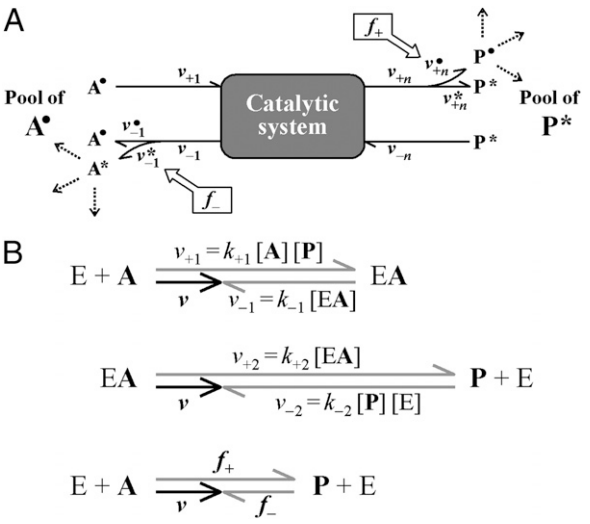

Fig. 3. Depiction of forward and back flux during the net reaction A → P in a steady state catalytic system with reversible but otherwise unknown internal reactions. Such a system can consist of an entire pathway (*A*) or a single enzymatic reaction (*B*; E + A → EA → P + E) (Figs. S4 and S5). All reactions, including uptake or binding and release, are reversible. Arrows indicate rates (velocities). The forward (v_+) and back (v_-) rates correspond to individual steps in a catalytic system. The index *n* refers to the number of forward and backward fluxes (*B*; *n* = 2 for a single enzymatic reaction) (Fig. S5). A description of abbreviations is given in Table S3. (*A*) Catalytic system: the fate of substrate and product is followed by the different labels (A•, P*) of the initial pools. Release of A and P includes both the returned fraction that never reached the other side ($v^\bullet_{-1}$, v^*_{+n}), and the fraction directly derived from the other side ($v^\bullet_{+n}$, v^*_{-1}). Forward (f_+) and back (f_-) flux are the concentrations (amounts per investigated volume) of P• and A* most recently derived per time from A• and P*, respectively. Hence, return to the side of their origin with progressing reaction is neglected by examining a short time interval (A* in A• and P• in P* remaining very dilute). (*B*) Vector model for individual rates during net rate (v) of a single enzymatic reversible reaction (E + A ⇄ EA ⇄ P + E) (Fig. S5) in a steady state (pools of A and P are essentially constant). The sizes of the rates are indicated by lengths of arrows. The same net rate (v) is the difference of uptake (binding) and release of substrate (v_{+1}, v_{-1}) and product (v_{+2}, v_{-2}) as well as the difference between forward and back flux (f_+, f_-). The rate constants for the reaction steps (k_{+1}, k_{-1}, k_{+2}, k_{-2}) and the actual concentrations of E, A, and P determine v_{+1}, v_{-1}, v_{+2}, v_{-2}, respectively, as indicated, and the resulting f_+, and f_-, which can only be revealed by labeling (Eqs. **S35** and **S36**). The vector model was calculated for an enzymatic reaction with (in rate units) $v_{+1} = 6$, $v_{-1} = 4$, $v_{+2} = 9$, $v_{-2} = 7$; result: $v = 2$, $f_+ = 4.15$, $f_- = 2.15$. The associated change in free energy (free energy dissipated) is $\Delta G = R\,T\ln(f_-/f_+) = -1.63$ kJ (mol A)$^{-1}$ (formula resulting from Eq. **8**; $T = 298$ K).

www.pnas.org/cgi/doi/10.1073/pnas.1218683109

BIOCHEMISTRY

Correction for "Protein pyrophosphorylation by inositol pyrophosphates is a posttranslational event," by Rashna Bhandari, Adolfo Saiardi, Yousef Ahmadibeni, Adele M. Snowman, Adam C. Resnick, Troels Z. Kristiansen, Henrik Molina, Akhilesh Pandey, J. Kent Werner, Jr., Krishna R. Juluri, Yong Xu, Glenn D. Prestwich, Keykavous Parang, and Solomon H. Snyder, which appeared in issue 39, September 25, 2007, of *Proc Natl Acad Sci USA* (104:15305–15310; first published September 14, 2007; 10.1073/pnas.0707338104).

The authors note that Figs. 1*b*, 1*d*, 1*g*, and 4*a* have been revised to include dividing lines between lanes to show where nonessential lanes were removed from a single original gel. Figs. 2*c*, 2*d*, and 3*c* have been revised to include boxes to indicate samples run on different gels, under the same conditions; these gels are aligned with respect to the indicated molecular weight markers. Figs. 4*b* and 4*c* have been revised to eliminate errors that occurred in the original version during file conversion. The changes were made to comply with the PNAS policy that requires dividing lines whenever entire nonessential lanes have been removed from a single original gel, and clear demarcation of samples run on separate gels. These changes do not affect the data presented nor the conclusions of the article. The corrected figures and their legends appear below.

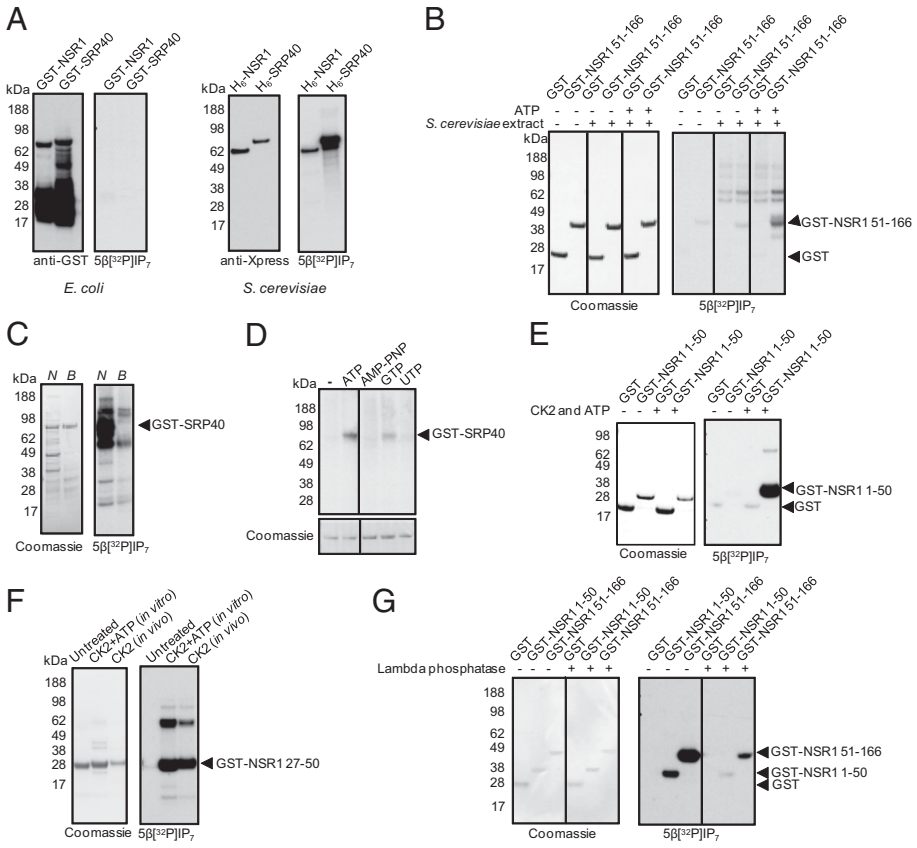

Fig. 1. IP_7-mediated protein phosphorylation requires prephosphorylation by protein kinases. (*a*) NSR1 and SRP40 purified from *E. coli* or *S. cerevisiae* were incubated with 5β[^{32}P]IP_7 and resolved by NuPAGE; immunoblotting with a tag-specific antibody (*Left*) and autoradiography to determine phosphorylation (*Right*). (*b*) GST or GST-tagged NSR1 fragment (amino acids 51–166) expressed in *E. coli* and immobilized on glutathione beads were preincubated with or without *S. cerevisiae* extract or ATP, washed with PBS, and then treated with 5β[^{32}P]IP_7 and resolved by NuPAGE; Coomassie brilliant blue R250 staining (*Left*) and autoradiography (*Right*). The extra phosphorylated protein bands in lanes 3–6 are yeast proteins that bound nonspecifically to glutathione beads. (*c*) GST-SRP40 purified from *E. coli* was preincubated with ATP and either native *S. cerevisiae* extract (*N*) or extract that had been boiled for 5 min (*B*) and then treated with 5β[^{32}P]IP_7 as in *b*. (*d*) GST-SRP40 purified from *E. coli* was preincubated with yeast extract and indicated nucleotides and then phosphorylated by 5β[^{32}P]IP_7;Coomassie brilliant blue R250 staining (*Lower*) and autoradiography (*Upper*). (*e*) GST or GST-tagged NSR1 fragment (amino acids 1–50) purified from *E. coli* were preincubated with or without CK2 and ATP and then treated with 5β[^{32}P]IP_7 as in *b*. (*f*) GST-tagged NSR1 fragment (amino acids 27–50) purified from *E. coli* was incubated without or with CK2 and ATP (lanes 1 and 2) or coexpressed in *E. coli* with the catalytic A1 subunit of human CK2 (lane 3). Purified proteins were incubated with 5β[^{32}P]IP_7 as in *b*. (*g*) GST or GST-tagged NSR1 fragments (amino acids 1–50 and 51–166) purified from *S. cerevisiae*, were preincubated in the absence or presence of λ-phosphatase and then phosphorylated by 5β[^{32}P]IP_7 as in *b*.

CORRECTIONS

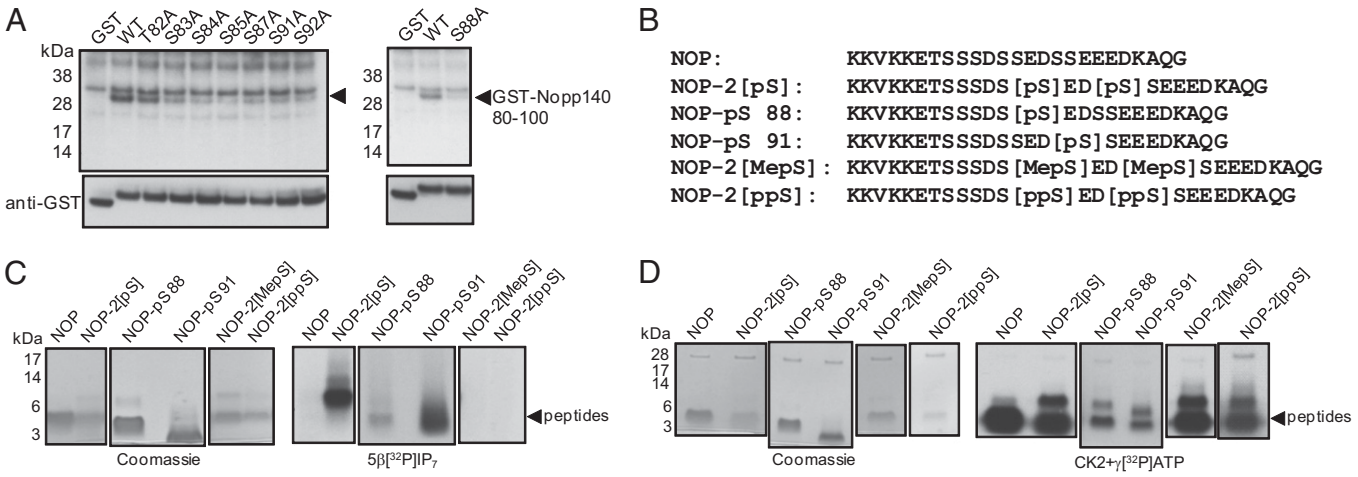

Fig. 2. IP_7 phosphorylates a phosphoserine residue to generate pyrophosphoserine. (*a*) Extracts from *S. cerevisiae* expressing GST-tagged mouse Nopp140 fragment (amino acids 80–100) WT sequence and indicated point mutants were phosphorylated by 5β[^{32}P]IP_7; autoradiography (*Upper*) and immunoblotting (*Lower*). (*b*) Sequences of individual peptides derived from Nopp140 (GenBank accession no. NP_941035). NOP, amino acids 76–100 of mouse Nopp140; NOP-2[pS], the same sequence as NOP except with phosphoserine at positions 88 and 91; NOP-pS 88 and NOP-pS 91, single phosphoserine residues at positions 88 and 91 respectively; NOP-2[MepS], methylphosphoserine at positions 88 and 91; NOP-2[ppS], pyrophosphoserine at positions 88 and 91. (*c* and *d*) The six synthetic peptides in *b* were incubated with 5β[^{32}P]IP_7 (*c*) or with CK2 and γ[^{32}P]ATP (*d*) and resolved by NuPAGE. Coomassie G250 staining (*Left*) and autoradiography (*Right*). In each peptide lane, there are multiple bands in the 3- to 9-kDa range, corresponding to peptide monomers and multimers, generated possibly because of electrostatic interactions between the positively charged lysines and negatively charged acidic and phosphate-containing residues (27). Peptide dimers were also observed by MALDI-TOF analysis (data not shown).

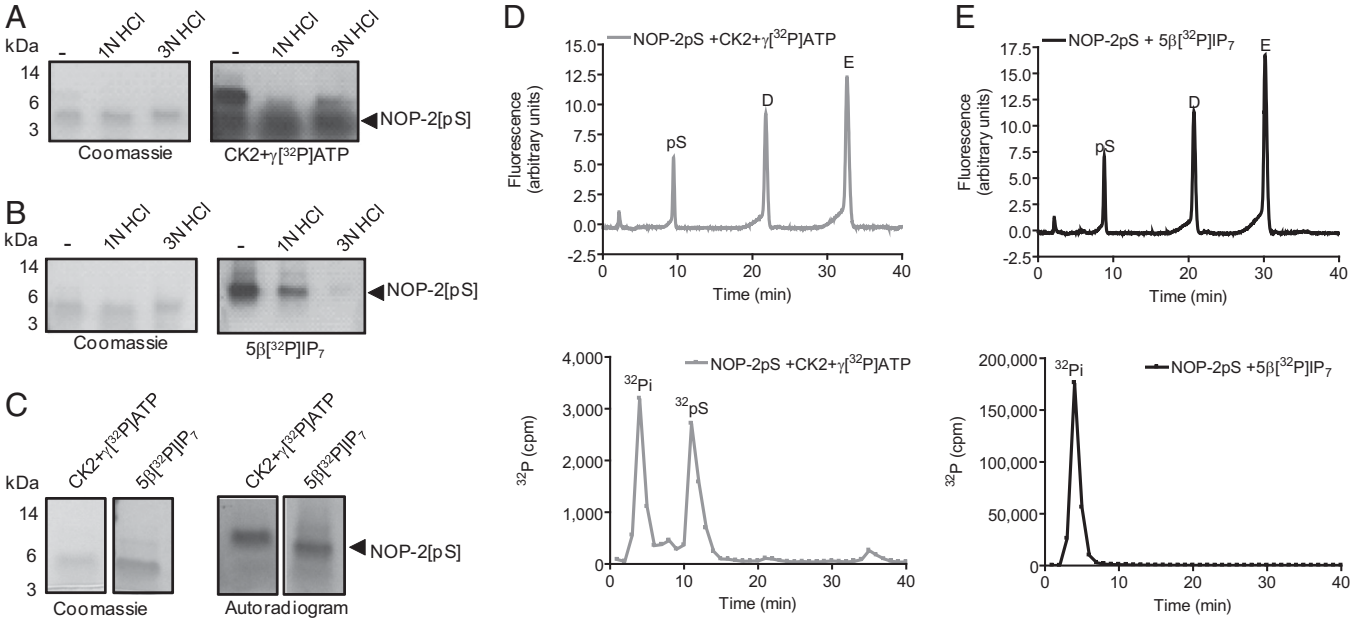

Fig. 3. The properties of pyrophosphoserine differ from those of phosphoserine. (*a* and *b*) NOP-2[pS] peptide was phosphorylated by CK2 and γ[^{32}P]ATP (*a*) or by 5β[^{32}P]IP_7 (*b*), then treated with HCl and subjected to NuPAGE; Coomassie G250 staining (*Left*) and autoradiography (*Right*). (*c*) NOP-2[pS] peptide was phosphorylated by either CK2 and γ[^{32}P]ATP or by 5β[^{32}P]IP_7 as described in *SI Materials and Methods*. A fraction of the phosphorylated peptides was subjected to NuPAGE to ensure equivalent phosphorylation under both conditions; Coomassie G250 staining (*Left*) and autoradiography (*Right*). (*d* and *e*) The remaining CK2 phosphorylated peptide (*d*) and IP_7-phosphorylated peptide (*e*) were hydrolyzed with 6 M HCl, and the resulting amino acids were resolved by HPLC. Data collected during the first 40 min of the HPLC run are presented; elution profiles of the first 3 aa (*Upper*) and corresponding radioactivity in each 1-ml fraction (*Lower*). Note that high levels of $^{32}P_i$ in the IP_7-phosphorylated sample compared with the CK2 and ATP phosphorylated sample are due to incomplete removal of 5β[^{32}P]IP_7 from the peptide during desalting (see *SI Materials and Methods*).

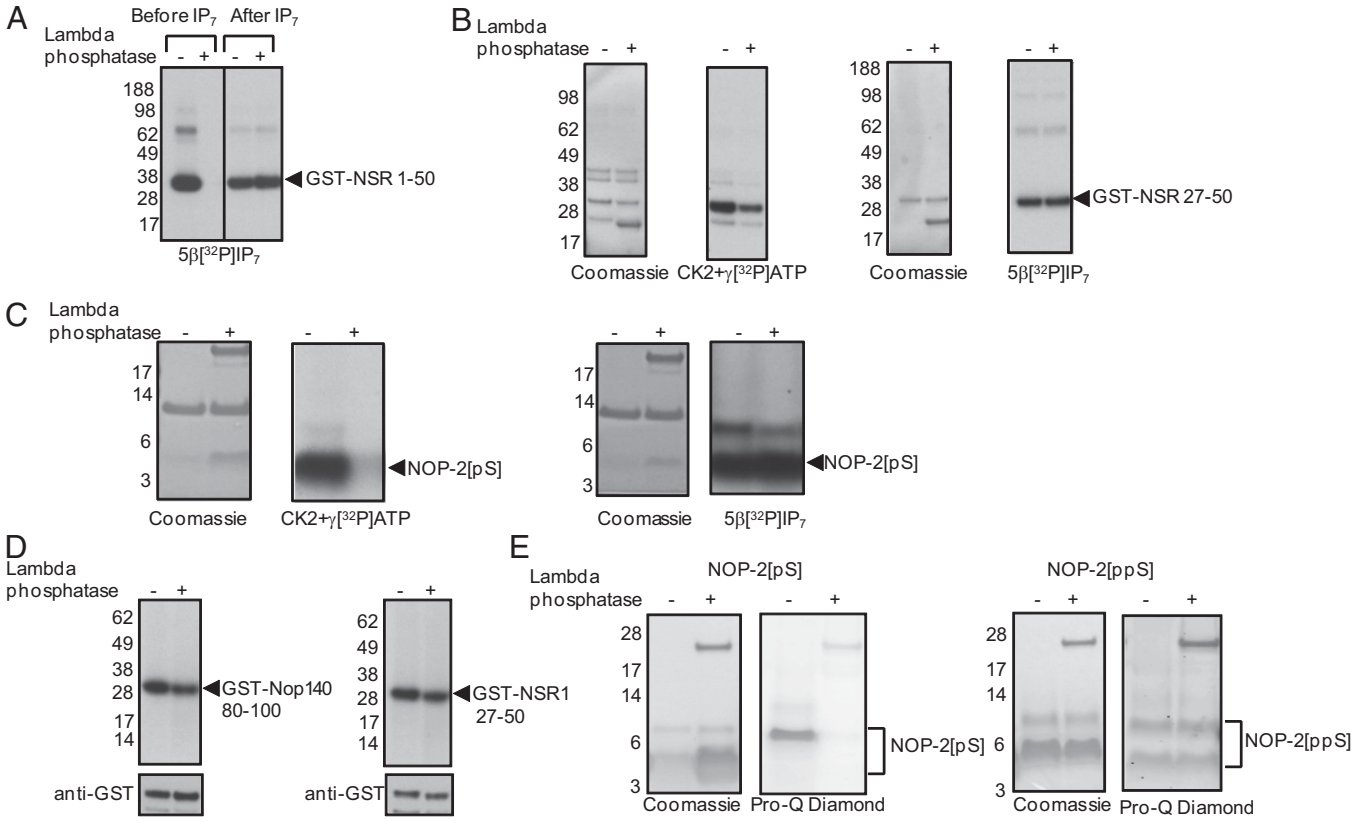

Fig. 4. λ-phosphatase does not dephosphorylate IP_7-phosphorylated proteins. (*a*) GST-tagged NSR1 fragment (amino acids 1–50) purified from *S. cerevisiae* was incubated without or with λ-phosphatase and then phosphorylated by 5β[^{32}P]IP_7 (lanes 1 and 2). Alternatively, the protein was first phosphorylated by 5β[^{32}P]IP_7 and then incubated without or with λ-phosphatase (lanes 3 and 4). The samples were resolved by NuPAGE and autoradiographed. (*b*) GST-tagged NSR1 fragment (amino acids 27–50) purified from *S. cerevisiae* was phosphorylated either by CK2 and γ[^{32}P]ATP (*Left*) or by 5β[^{32}P]IP_7 (*Right*) and then incubated with or without λ-phosphatase; Coomassie G250 staining (*Left*) and autoradiography (*Right*). (*c*) NOP-2[pS] peptide bound to streptavidin agarose beads was phosphorylated by either CK2 and γ[^{32}P]ATP (*Left*) or by 5β[^{32}P]IP_7 (*Right*) and then incubated with or without λ-phosphatase as in *b*. (*d*) *S. cerevisiae* expressing GST-tagged Nopp140 fragment (amino acids 80–100) (*Left*) or NSR1 fragment (amino acids 27–50) (*Right*) were labeled with inorganic orthophosphate [$^{32}PO_4]_i$. Purified radiolabeled proteins were incubated with or without λ-phosphatase; autoradiography (*Upper*) and immunoblotting (*Lower*). (*e*) NOP-2[pS] peptide (*Left*) or NOP-2[ppS] peptide (*Right*) were treated with or without λ-phosphatase, resolved by NuPAGE, and stained with either Coomassie G250 or Pro-Q Diamond phosphoprotein gel stain, as indicated.

www.pnas.org/cgi/doi/10.1073/pnas.1218152109

Carbon and sulfur back flux during anaerobic microbial oxidation of methane and coupled sulfate reduction

Thomas Holler[a], Gunter Wegener[a], Helge Niemann[a,b], Christian Deusner[a,1], Timothy G. Ferdelman[a], Antje Boetius[a,c], Benjamin Brunner[a,2], and Friedrich Widdel[a]

[a]Max Planck Institute for Marine Microbiology, Laboratories for Microbiology, Biogeochemistry, and Microbial Habitats, 28359 Bremen, Germany; [b]Institute for Environmental Geosciences, University of Basel, 4056 Basel, Switzerland; and [c]Alfred Wegener Institute for Polar and Marine Research, Research Group for Deep Sea Ecology and Technology, 27515 Bremerhaven, Germany

Edited by Donald E. Canfield, University of Southern Denmark, Odense M., Denmark, and approved November 1, 2011 (received for review April 22, 2011)

Microbial degradation of substrates to terminal products is commonly understood as a unidirectional process. In individual enzymatic reactions, however, reversibility (reverse reaction and product back flux) is common. Hence, it is possible that entire pathways of microbial degradation are associated with back flux from the accumulating product pool through intracellular intermediates into the substrate pool. We investigated carbon and sulfur back flux during the anaerobic oxidation of methane (AOM) with sulfate, one of the least exergonic microbial catabolic processes known. The involved enzymes must operate not far from the thermodynamic equilibrium. Such an energetic situation is likely to favor product back flux. Indeed, cultures of highly enriched archaeal–bacterial consortia, performing net AOM with unlabeled methane and sulfate, converted label from ^{14}C-bicarbonate and ^{35}S-sulfide to ^{14}C-methane and ^{35}S-sulfate, respectively. Back fluxes reached 5% and 13%, respectively, of the net AOM rate. The existence of catabolic back fluxes in the reverse direction of net reactions has implications for biogeochemical isotope studies. In environments where biochemical processes are close to thermodynamic equilibrium, measured fluxes of labeled substrates to products are not equal to microbial net rates. Detection of a reaction in situ by labeling may not even indicate a net reaction occurring in the direction of label conversion but may reflect the reverse component of a so far unrecognized net reaction. Furthermore, the natural isotopic composition of the substrate and product pool will be determined by both the forward and back flux. This finding may have to be considered in the interpretation of stable isotope records.

element cycle | anaerobic methanotrophy | biological thermodynamics | Haldane relationship

Microbial catabolic pathways and their rates in habitats and cultures are frequently measured by adding isotopically labeled substrate and quantifying the rate of label appearance in the product pool. Such label flux is usually regarded as unidirectional and thus, assumed to represent the rate of substrate conversion. However, in enzyme kinetics, like in chemical kinetics, the concept of bidirectionality or reversibility of biochemical reactions is a long-established feature (1–5).* Hence, if substrate is converted to product through a multistep pathway and each reaction occurs with a back reaction, some steady flux of the terminal product by intermediate pools back to the substrate pool should occur. Such back flux is measurable by isotope labeling of the product and measuring label appearance in the vanishing substrate pool. This finding would, in principle, be analogous to the established measurement of isotope exchange to gain insights into basic enzyme mechanisms (1–5).

Like in enzymatically catalyzed single reactions, one expects that the back flux through the entire chain (sequence) of individual catabolic reactions should be more significant the less exergonic the overall reaction becomes, because an individual reaction within the sequence cannot be more exergonic (more irreversible) than the overall reaction. A weakly exergonic catabolism (energy metabolism) is common in strictly anaerobic microorganisms (6–11). Still, the possibility of product back flux in anaerobes has been largely neglected and treated only in relatively few labeling studies. The perhaps best-known example is the conversion of added ^{14}C-methane to ^{14}C-carbon dioxide during net methane formation by various methanogenic archaea (12–16). The enzymatic key reaction of this back flux, the methyl carbon exchange between added $^{13}CH_4$ and its direct precursor $^{12}CH_3$-coenzyme M, was recently quantified in an enzymatic assay, with all reaction partners present at equilibrium concentrations (that is, without net methane formation or consumption) (17). Furthermore, conversion of added ^{35}S-sulfide to ^{35}S-sulfate during net reduction with lactate by *Desulfovibrio* has been observed (18). The incorporation of added $^{14}CO_2$ into the carboxyl group of acetate during oxidation through the Wood–Ljungdahl (carbon monoxide dehydrogenase) pathway in an anaerobe is an example of partial product back flux (19, 20).

These studies indicate reversibility and operation close to thermodynamic equilibrium of specific substrate–product reaction sequences within an overall catabolism (that encompasses electron acceptor and donor). Here, we show reversibility of an entire anaerobic catabolism, including electron donor as well as the electron acceptor, and present a refined quantitative data evaluation to reveal the extent of back flux. The examined process is the anaerobic oxidation of methane with sulfate (AOM) (**1**),

$$CH_4(g) + SO_4^{2-} \rightarrow HCO_3^- + HS^- + H_2O \qquad [1]$$

which is energetically characterized by (Eq. **2**)

$$\Delta G^\circ = -16.6 \text{ kJ mol}^{-1}, \quad \frac{\{HCO_3^-\}\{HS^-\}}{\{CH_4(g)\}\{SO_4^{2-}\}} = 10^{2.9} \qquad [2]$$

and thus one of the least exergonic processes sustaining life (ΔG in situ is often between −20 and −40 kJ mol^{-1}) (21–23). It should, therefore, be associated with noticeable reversibility. AOM is of great environmental significance, because it counteracts

Author contributions: T.H. and F.W. designed research; T.H. and H.N. performed research; T.H., C.D., and T.G.F. contributed new reagents/analytic tools; T.H., H.N., T.G.F., B.B., and F.W. analyzed data; and T.H., G.W., T.G.F., A.B., B.B., and F.W. wrote the paper.

The authors declare no conflict of interest.

This article is a PNAS Direct Submission.

[1]Present address: Leibniz Institute of Marine Sciences, University of Kiel, 24148 Kiel, Germany.

[2]To whom correspondence should be addressed. E-mail: bbrunner@mpi-bremen.de.

See Author Summary on page 20869.

This article contains supporting information online at www.pnas.org/lookup/suppl/doi:10.1073/pnas.1106032108/-/DCSupplemental.

*The existence of an enzyme catalyzing only one direction of an essentially reversible reaction (and not gaining energy from another source or not undergoing a permanent change) may be falsified as follows. If such an enzyme existed, its addition to a system in which concentrations of reactant (A) and product (P) have reached the thermodynamic equilibrium ($\Delta G = 0$ for A ⇌ P) would cause a spontaneous shift away from the equilibrium. Such a reaction valve (a variant of Maxwell's demon) would be in conflict with the second law of thermodynamics.

methane release from marine sediments into the oxic biosphere (refs. 24 and 25 and references therein). It is catalyzed by consortia of phylogenetically distinct Euryarchaeota [anaerobic methanotrophs (ANME groups)] and associated Deltaproteobacteria; the latter are assumed to perform sulfate reduction (26–30). Labeling studies using natural sediment samples with AOM activity provided hints of $^{14}CO_2$ conversion to $^{14}CH_4$ during net AOM by the indigenous consortia (31–33). The mode of coupling, which does not seem to involve conventional anaerobic intermediates such as H_2 or acetate, remains a matter of discussion (*SI Text, Anaerobic Oxidation of Methane as Enzymatically Catalyzed System* and Fig. S1) (21, 23, 34–37).

Axenic AOM consortia have not been isolated so far. To clearly show reversibility of AOM and exclude microbial use of substrates other than methane and sulfate, we used essentially detritus-free marine AOM consortia that had been highly enriched by repeated transfer and growth with CH_4 and SO_4^{2-} as the only added energy source.

Results

Characterization of Enriched AOM Cultures. The sediment-free, methane-consuming, and sulfide-producing enrichment cultures were first characterized with respect to the occurring phylotypes and unequivocal AOM activity to verify suitability for the isotope back flux studies. The abundant cells were archaea (ANME-2 groups) and Deltaproteobacteria (95–99% of detectable cells according to DAPI and specific 16S rRNA probing) (38, 39). Specific (dry mass related) activities for methane consumption and sulfide formation were ~0.3 and 2.0 mmol g^{-1} d^{-1} in the Hydrate Ridge (HR) and Isis Mud Volcano (MV) enrichment cultures, respectively (39). Substrate labeling experiments with $^{14}CH_4$ and $^{35}SO_4^{2-}$ and product label quantification performed in this study yielded a molar ratio between formed CO_2 and H_2S of 0.96/1 (HR) and 1.07/1 (MV) in accordance with expression **1**[†] (Table S1). From previous chemical analysis of incubations without methane, it is known that net methane production is marginal (i.e., <0.05% of the AOM rate) (39). The rate of net sulfide production without methane was <5% of the rate achieved in the presence of methane (Table S2). This finding showed that background methanogenesis and sulfate reduction with endogenous compounds, residual detrital matter, or dead cell carbon were essentially absent or very small, respectively. These cultures were, therefore, ideal to study the flux of labeled inorganic carbon and sulfide into the pools of methane and sulfate, respectively, when these compounds were present as substrates.

Sulfur and Carbon Back Fluxes. For convenience, product label back fluxes during net AOM were determined as rates relative to the culture volumes (rather than to biomass). Increase in sulfide concentration yielded methane-dependent sulfate reduction rates of 190 μmol L^{-1} d^{-1} (MV) (Fig. 1*A*) and 120 μmol L^{-1} d^{-1} (HR) (*SI Text, Time Course Experiment with Consortia from Hydrate Ridge* and Fig. S2*A*). In experiments with labeled sulfide, the overall ^{35}S activity was constant during the whole time series. Increasing amounts of tracer were recovered in the $^{35}SO_4^{2-}$ pool of AOM-active samples. However, in contrast to constant sulfate reduction rates (Fig. 1*A* and Fig. S2*A*), label transfer from the sulfide to the sulfate pool decreased during the course of the experiment because of the significant dilution of the ^{35}S-sulfide label with steadily forming unlabeled sulfide (Fig. 1*B* and Figs. S2*B* and S3). This dilution was taken into consideration by refined data evaluation (*Materials and Methods* and *SI Text, Calculation of Reverse Reaction Rate*). The determined rates of sulfur back flux were 7% and 13% (HR and MV, respectively) of the AOM rate based on chemical quantification (Figs. 1*C* and 2, Fig. S2*C*, and Table S2). The flux of ^{35}S label from the sulfide to the sulfate pool was negligible when AOM was prevented by omission of methane (Fig. 1*B* and Fig. S2*B*).

The calculated rates of the back flux of dissolved inorganic carbon (DIC; CO_2, HCO_3^-, and CO_3^{2-}) to methane (DIC → CH_4) were 3.2% and 5.5% (HR and MV, respectively) of the net AOM rate (Fig. 2 and Table S1). This finding is at least one order of magnitude higher than the methane–carbon back flux (CH_4 → DIC) during net methanogenesis in methanogenic cultures (0.001–0.36%) (12–14). The ratios between sulfur and carbon back fluxes were 2.2 and 2.4 (HR and MV, respectively) and thus, nearly identical for the two enrichment cultures. We also measured the flux of ^{14}C label from the inorganic carbon pool to methane, whereas the net oxidation reaction was prevented by omission of sulfate in the presence of methane. Label from ^{14}C-inorganic carbon still appeared in the methane pool at rates of 2.4% and 2.3% (HR and MV, respectively) of the AOM rate with sulfate (Table S1).

Discussion

As expected, our ^{35}S- and ^{14}C-labeling results clearly showed substantial fluxes of sulfide back to sulfate and bicarbonate back to methane during AOM, and they confirm the reversibility of an entire catabolic process with low-energy yield. Such catabolic reversibility is viewed from a more general kinetic and thermodynamic perspective with respect to implications in the biogeochemical study of in situ catabolic rates and isotope patterns of biologically redox-active elements.

Concept of Catabolic Back Flux. A catabolic pathway in cells of a prokaryotic species or community represents a complex sequence of many enzymatic reactions and intermediates (intercellular; in communities, they are also extracellular). If the subsequent reactions occur with reversibility and are viewed from the molecular perspective (that is, regarding microstates stochastically) at a given moment, the larger fraction of the enzyme molecules of each reaction performs the forward reaction, whereas a smaller fraction simultaneously performs the reverse reaction. The resulting macrostate is a system with substrate uptake and reoutput and product output and reuptake. For convenience, this finding is illustrated in Fig. 3 for a simple overall reaction, A ⇌ P, with indication of the rates (v) and label (*) added to the product pool; the unlabeled ($^\bullet$) element is also indicated. Substrate reoutput (v_{-1}) not only includes the part derived from product (v^*_{-1}) but also substrate that never reached the product side ($v^\bullet_{-1}$). In a steady state, the sum of the uptake rates must equal the sum of the release rates (i.e., $v_{+1} + v_{-n} = v_{-1} + v_{+n}$), which leads to the net rate v (Eq. **3**):

$$v_{+1} - v_{-1} = v_{+n} - v_{-n} = v. \quad [3]$$

The rates of substrate formation from product (v^*_{-1}) and product formation from substrate ($v^\bullet_{+n}$) are experimentally accessible by isotope labeling. For better distinction, we designate these particular rates $v^\bullet_{+n} = f_+$ and $v^*_{-1} = f_-$. Net disappearance of substrate, $v = v_{+1} - v^\bullet_{-1} - f_-$, and mass conservation, $v_{+1} - v^\bullet_{-1} = f_+$, yield for the net rate (Eq. **4**)

$$v = f_+ - f_-. \quad [4]$$

Hence, the net rate is expressed by three pairs of rates (Eqs. **3** and **4**; for single enzyme shown in Fig. 3*B*), with f_+, f_-, and v being experimentally accessible. During net reaction A → P, there are the inequalities (**5** and **6**)

$$v_{+1}, v_{+n} > f_+ > v \quad [5]$$

and

[†]Like with chemical quantification (21), such labeling experiments are not precise enough to reveal the proportion of methane–carbon channeled into biosynthesis as deviation from the 1:1 stoichiometry, because only around 1% of consumed methane is assimilated (38).

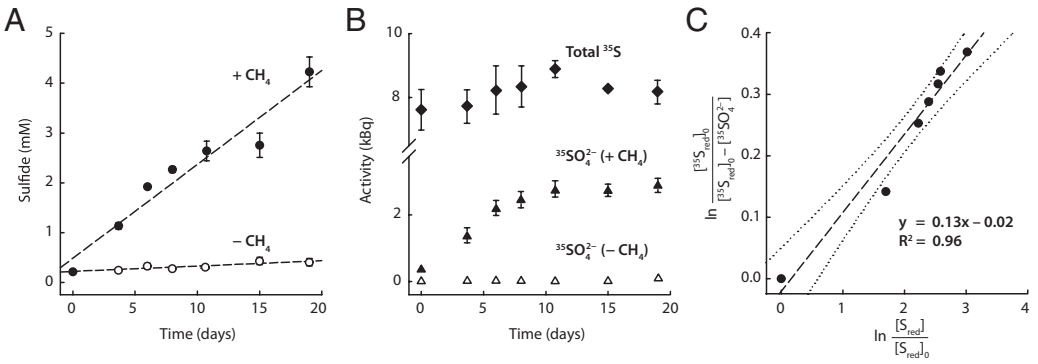

Fig. 1. Time course experiment: the addition of labeled sulfide (product) to highly enriched, detritus-free consortia from Isis MV that perform anaerobic oxidation of methane. (*A*) Developing sulfide concentrations in the presence (●) and absence (○) of methane. (*B*) Development of ^{35}S-activity in the sulfate pool during incubation with (▲) and without (△) methane as electron donor. The total ^{35}S-activity (◆, sulfate + sulfide) is also indicated. The shown radiolabel was determined after incubation at the same time to eliminate the effect of decay. (*C*) Double logarithmic plot according to Eq. **16** to calculate the reverse rate; dotted line marks the 95% confidence interval.

$$f_+ > f_- . \qquad [6]$$

Flux Rates and Free Energy. Thermodynamic values such as free energies are based on macroscopic time-independent equilibria, and they cannot, in principle, predict reaction rates, which are determined by molecular mechanisms. However, the actual free energy change (more precisely, the change in chemical potential) and rate of a reaction are both determined (at constant temperature) by concentrations (strictly speaking, by activities in the case of chemical potentials). The thermodynamic and kinetic treatment of a reaction must, therefore, meet each other at equilibrium, where the free energy as well as the net reaction rate (resulting from concentration-dependent forward and back reaction) is zero. This connection[‡] has been a basic aspect in enzyme kinetics (1, 3–5, 40). A similar analytical treatment of the connection between energetics and kinetics of the here investigated microbial catabolic system is presently impossible in view of its complexity and the largely unknown enzymes and intermediates. To substantiate the initial argument that the reverse flux must increase relatively with decreasing free energy, we present this connection for a simple enzymatic reaction, again formulated with one substrate, A, and one product, P. Furthermore, only a lumped enzyme-bound state, EA, appears in the reaction (Fig. 3 and *SI Text, Thermodynamics and Kinetics in Catabolism*); kinetic constants are designated as k.

As for a reversible, two-step purely chemical reaction, formulation of equilibrium conditions (*SI Text, Thermodynamics and Kinetics in Catabolism*) yields $k_{+1}k_{+2}/(k_{-1}k_{-2}) = [P]_e/[A]_e$ (the parameters $[P]_e$ and $[A]_e$ indicate concentrations at equilibrium). This leads to the Haldane relationship. Its common formulation includes the experimentally accessible Michaelis (composite) constants $K_{m+} = (k_{-1} + k_{+2})/k_{+1}$ and $K_{m-} = (k_{-1} + k_{+2})/k_{-2}$ for the forward and reverse reactions, respectively, which are obtained through multiplying nominator and denominator with $k_{-1} + k_{+2}$. By designating $k_{+2} = k_{cat+}$ and $k_{-1} = k_{cat-}$ (catalytic constants for product and substrate formation, respectively) and expressing the equilibrium constant, K_e, through the standard free energy change, ΔG° (*SI Text, Thermodynamics and Kinetics in Catabolism*), the Haldane relationship can be expressed as (Eq. **7**)

$$\frac{k_{+1}k_{+2}}{k_{-1}k_{-2}} = \frac{k_{cat+}/K_{m+}}{k_{cat-}/K_{m-}} = \frac{[P]_e}{[A]_e} = K_e = e^{-\Delta G^\circ/(RT)}. \qquad [7]$$

A certain imprecision lies in the fact that concentrations (in kinetics) and activities (in thermodynamics) are treated here as numerically equivalent.

Under nonequilibrium conditions, the net reaction rate $v \neq 0$ results from the individual rates or fluxes (Eq. **3** or **4**, respectively), which are determined by the actual concentrations, [A] and [P], and the kinetic rate constants, k_{+1}, k_{+2}, k_{-1}, and k_{-2}. The latter again are connected by Eq. **7**. [A] and [P] also determine the actual free energy, $\Delta G < 0$. This finding leads to a connection between the flux ratio, f_- and f_+, and the actual free energy (where the standard free energy, ΔG°, no longer appears; derivation in *SI Text, Thermodynamics and Kinetics in Catabolism*) (Eq. **8**):

$$\frac{f_-}{f_+} = \frac{k_{-1}k_{-2}[P]}{k_{+1}k_{+2}[A]} = \frac{[P]}{K_e[A]} = e^{\Delta G/(RT)}. \qquad [8]$$

With Eq. **4**, the back flux can be also related to the net rate (Eq. **9**):

$$\frac{f_-}{v} = \frac{1}{K_e[A]/[P] - 1} = \frac{1}{e^{-\Delta G/(RT)} - 1}. \qquad [9]$$

Eqs. **8** and **9** express that forward and back flux catalyzed by an enzyme at given substrate and product concentrations cannot vary

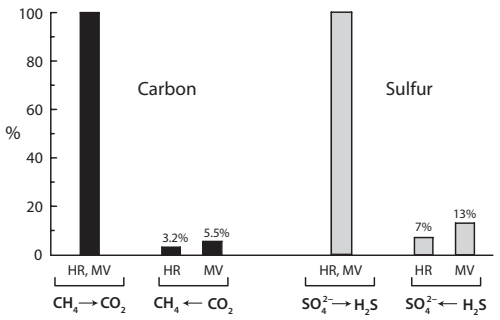

Fig. 2. Comparison of reverse (back flux) to net reactions (set to 100%) during the anaerobic oxidation of methane with sulfate by highly enriched consortia from HR and Isis MV. Data analysis underlying sulfur back flux is in Fig. 1.

[‡]Sometimes, this connection is somewhat erroneously termed thermodynamic constraint of reaction kinetics or described as thermodynamics governing kinetics.

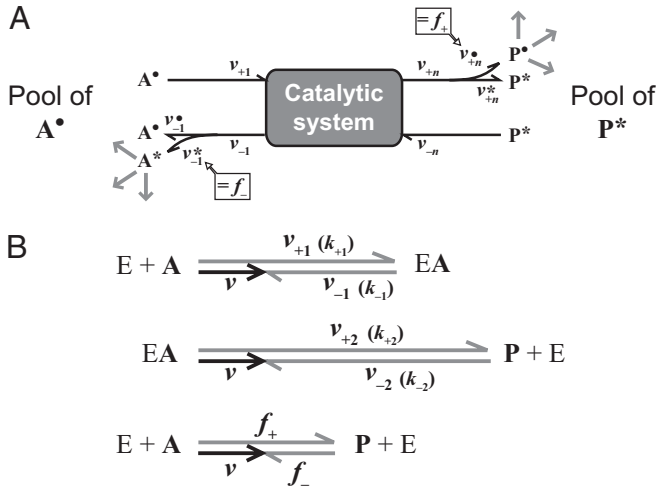

Fig. 3. Depiction of forward and back flux during the net reaction A → P in a steady state catalytic system with reversible but otherwise unknown internal reactions. Such a system can consist of an entire pathway (*A*) or a single enzymatic reaction (*B*; E + A → EA → P + E) (Figs. S4 and S5). All reactions, including uptake or binding and release, are reversible. Arrows indicate rates (velocities). The forward (v_+) and back (v_-) rates correspond to individual steps in a catalytic system. The index n refers to the number of forward and backward fluxes (*B*; $n = 2$ for a single enzymatic reaction) (Fig. S5). A description of abbreviations is given in Table S3. (*A*) Catalytic system: the fate of substrate and product is followed by the different labels (A•, P*) of the initial pools. Release of A and P includes both the returned fraction that never reached the other side ($v^\bullet_{-1}$, v^*_{+n}), and the fraction directly derived from the other side ($v^\bullet_{+n}$, v^*_{-1}). Forward (f_+) and back (f_-) flux are the concentrations (amounts per investigated volume) of P• and A* most recently derived per time from A• and P*, respectively. Hence, return to the side of their origin with progressing reaction is neglected by examining a short time interval (A* in A• and P• in P* remaining very dilute). (*B*) Vector model for rates in a single enzymatic reaction (E + A → EA → P + E) (Fig. S5). The sizes of rates are indicated by lengths of arrows. The same net rate (v) is the difference of uptake (binding) and release of substrate (v_{+1}, v_{-1}) and product (v_{+2}, v_{-2}) as well as the difference between forward and back flux (f_+, f_-). The rate constants for a single enzymatic reaction, k_{+1}, k_{-1}, k_{+2}, k_{-2}, and the actual concentrations determine v_{+1}, v_{-1}, v_{+2}, v_{-2}, respectively. The vector model was calculated for the enzymatic reaction using (in rate units): $v_{+1} = 6$, $v_{-1} = 4$, $v_{+2} = 9$, $v_{-2} = 7$; result: $v = 2$, $f_+ = 4.15$, $f_- = 2.15$ (Eqs. S35 and S36).

independently of each other (because the kinetic constants cannot vary independently) (Eq. **7**). The equations also show that the back flux relative to the forward flux or net rate becomes the more relevant the closer the reacting system is to the thermodynamic equilibrium. Marginal to essentially no back flux can only be expected for strongly exergonic linear reaction sequences (very negative ΔG).

Remarks on Back Flux Through an Entire Catabolism with Special Reference to AOM. Accordingly, relevant product back flux is expected in microbial cells or cell communities catalyzing cascades of enzymatic reactions through a weakly exergonic catabolism. A catabolism operating not far from the thermodynamic equilibrium can only include reactions that are at least as close to the equilibrium [that is, that cannot be strongly energy-dissipating (irreversible)]. The process in our experiments, AOM, is one of the least exergonic catabolic processes. Under the incubation provided in this study, the calculated free energy change (21) for AOM is only −25 to −35 kJ mol^{-1}. The range in natural habitats is often −20 to −40 kJ mol^{-1} (22, 23). The free energy actually dissipated by the in vivo catabolism is less negative than these calculated values because of coupling to energy conservation. Such coupling may be an important factor contributing to catabolic reversibility and back flux. Largely irreversible, energy-dissipating reactions during AOM are expected only in the anabolism (biosynthesis).

Sulfur back flux was at least two times as fast as carbon back flux during AOM. This finding shows that back fluxes (and forward fluxes) of electron acceptor and electron donor are not necessarily stoichiometrically coupled. This finding is in contrast to the ratio of their net rates, which in a steady state must always reflect the overall stoichiometry. Hence, the pathways of the electron acceptor and electron donor may be differently close to the equilibrium. This finding is analogous to enzymatic reactions with two (or more) substrates and two (or more) products, where isotope exchange rates may differ between substrate–reactant pairs depending on their mechanisms and individual rate constants (3, 4).

The extent of the relative reverse reactions in the 20 °C (293 K; MV) enrichment was higher than in the 12 °C (285 K; HR) enrichment (Fig. 2). Because the equilibrium constant, K_e (T, p), and hence also free energy change of a reaction (at given concentrations) are temperature-dependent, the extent of the reverse reaction relative to the forward or net reaction must be generally influenced by temperature. A thermodynamic prediction of this tendency is appealing. The equilibrium constants at two different temperatures (indices 1 and 2; $T_2 > T_1$) can be related to each other by (Eq. **10**)

$$\ln\frac{K_{e(2)}}{K_{e(1)}} = \frac{\Delta H^\circ}{R}\left(\frac{1}{T_1} - \frac{1}{T_2}\right), \qquad [10]$$

where ΔH° is the standard enthalpy change of the reaction.[¶] With $\Delta H^\circ = -11.4$ kJ mol^{-1} (assumed to be the same for 285, 293, and 298 K) for AOM, the ratio of the equilibrium constant of AOM at the two temperatures in this study is $K_{e(293\ K)}/K_{e(285\ K)} = 0.88$ (that is, <1). The extent of the reverse reactions is inversely proportional to the equilibrium constants (Eqs. **8** and **9**). Therefore, the extent of the reverse reactions of AOM at higher temperature to the extent at a lower temperature should be >1 (that is, reversibility should indeed increase with temperature). Still, a more refined quantitative treatment is presently not possible, because the catabolic reaction of AOM (**1**) is composed of sequential and parallel reactions. The above ΔH° is that of net AOM, whereas the enthalpies of the pathways of carbon and sulfur that constitute AOM and were examined separately as bulk reactions in this study are unknown.

Microbial Substrate–Product Interconversion Without Net Reaction? Enzymes continue catalyzing the forward and back reaction also when the equilibrium is reached (that is, if the net reaction is $v = 0$). This principle was recently applied to show methyl incorporation from $^{13}CH_4$ into methyl-coenzyme M by the purified terminal enzyme of methanogenesis (17). Hence, also multiple enzyme systems like microbial cells should catalyze interconversion of substrates and products (that is, exchange of labeled elements between them) in the absence of a net reaction. Indeed, when in our experiments methane and inorganic carbon were present whereas sulfate was essentially depleted so as to prevent net AOM, carbon back flux was still observed, albeit at a lower rate than during net AOM. However, if vice versa sulfate and

[¶]Derived from the fundamental equation (Eq. S56) (Eq. **11**)

$$\frac{\partial}{\partial T}\ln K_e = \frac{\Delta H^\circ}{RT^2}, \qquad [11]$$

expressing that $K_e = [A]/[P]$ increases with temperature for endothermic reactions ($\Delta H^\circ > 0$) and decreases for exothermic reactions ($\Delta H^\circ < 0$; Le Chatelier's principle). If we assume that ΔH° is temperature-independent within the small temperature range relevant in the present study (285 and 293 K; that is, without consideration of heat capacities of reactants and products), integration from $K_{e(1)}$, T_1 to $K_{e(2)}$, T_2 yields Eq. **10**.

sulfide were present without methane addition, sulfur label exchange was not observed. One explanation for the latter observation could be that sulfide back flux at low concentrations as prevailing in this particular experiment is a first-order process, allowing only marginal, barely detectable label back flux. Another explanation could be that arrest of the net reaction results in the depletion or inactivation of a coreactant or another component needed for an operative sulfur pathway. Forward and backward fluxes through intact in vivo systems are certainly more delicate than through a single enzymatic reaction, and understanding of the possibilities and conditions of substrate–product interconversion through various microbial pathways requires more detailed physiological investigations.

Consideration of Product Back Flux in Natural Habitats. Many environmentally relevant and microbial-mediated chemical reactions occur close to equilibrium conditions. Our findings have implications for studies of environmental processes at low-energy yields (for instance, in anoxic systems such as AOM environments or the deep biosphere). Microbial catabolic activity in natural habitats is often measured by examining the flux of added isotope label from substrate to product pool rather than by determining the net rate of product accumulation by chemical quantification. Tracer conversion rates in the opposite of net AOM or net methanogenesis have been reported from experiments with marine sediments (31, 33), bacterial mats (32), and methanogenic sludge (16, 41); however, these studies could not exclude the possibility of co-occurrence of methanogenesis and AOM. If back flux occurs, label flux from substrate will not be identical to the microbial net rate. In most cases, this effect (5–10%) will be hidden in the normal uncertainty and variability of radiotracer measurements. However, highly accurate net rate determination by isotope labeling would have to include both forward and back flux measurement to yield the net rate. Moreover, detection of a reaction in situ by labeling does not necessarily indicate a net reaction occurring in the direction of label conversion; it may represent the back flux during the opposite reaction and thus, a pseudoreaction; hence, dominance of the opposite reaction would have to be excluded, which was extensively discussed for methanogenesis vs. AOM (23). Nevertheless, as in biochemical studies of single enzyme reactions (17, 42), isotope probing of back fluxes at near equilibrium conditions may provide means of probing catabolic mechanisms at the community level.

Finally, reverse reactions are important also for the understanding of stable isotope fractionation (43–45). So far, the reversibility of sequential individual catabolic reactions but not the reversibility of an entire catabolism as a whole has been examined in isotope fractionation studies (18, 43, 46–49) (i.e., at least one step in a sequence of catabolic reactions was considered to be unidirectional). This treatment allowed determination of isotope effects according to a Rayleigh isotope fractionation equation. However, if an entire sequence of catabolic reactions is reversible, which it must be near equilibrium, the Rayleigh treatment is no longer valid, because the isotope composition of the reaction product (e.g., sulfide) affects the isotope composition of the reactant (e.g., sulfate). In the case of sulfate reduction, this effect has recently been observed in laboratory culture experiments (50). Our study and a recent study where discrepancies between bulk sulfate reduction rates and ^{35}S transfer from sulfate to sulfide were found (51) show that isotope fractionation between a reactant and a product under in situ conditions (e.g., AOM) may not be determined solely by kinetic isotope fractionation but also by the isotope composition of the product pool. A specific case of such bidirectional isotope fractionation may be that absence of net reaction could result in an equilibrium isotope fraction that reflects the highest thermodynamic stability of the involved isotopologues. Recent studies on pure cultures of sulfate reducing Bacteria indeed show that sulfur isotope fractionations approach equilibrium isotope fractionation values (52), implying that isotope exchange between product and substrate pools may, rather, be the rule than the exception for metabolism under low-energy condition. Refined measurements of isotope fractionations, which may also depend on the type of microorganisms (39), would be needed to explore the significance of the reverse reaction for stable isotope signatures under different settings of environmental and chemical parameters.

Materials and Methods

Origin, Enrichment, and Preparation of Cultures for Experiments. The investigated enrichment cultures originated from anoxic sediment of two marine methane seep areas, HR (Cascadia Margin, Oregon, NE Pacific; 044° 34.2′N, 125° 08.7′W; August 2000) and Isis MV sediment (Eastern Mediterranean Sea; 032° 21.7′N, 031° 23.4′E; September 2003). Sediments had been sampled during the *R/V Sonne* (SO-148/1, 2000) and *R/V L'Atalante* (NAUTINIL, 2003) expeditions, respectively. The methane-consuming, sulfide-producing cultures were enriched in anoxic synthetic seawater medium (53), with methane and sulfate as the only energy sources through repeated transfer (over some years) from sediment. Thereby, loosely flocculating cell aggregates were propagated, whereas the sediment matrix with detritus was continuously diluted out (confirmed by microscopic survey and microbial staining). Consortia of Archaea (ANME-2 groups) and Deltaproteobacteria were abundant (95–99% of detectable cells according to DAPI and specific 16S rRNA probing) (38, 39). These highly enriched consortia with their inherently slow growth (38) were available only in limited quantities and therefore, were used sparingly. Subsequently, experiments with ^{14}C-bicarbonate and ^{35}S-sulfide labeling were carried out at different times, and the batches available at one time differed from the batches at another time with respect to cell density and volumetric activity. Within an experiment at a given time, however, the same enrichment batch was distributed equally to establish equal volumetric activities. Before the radiotracer studies, cultures were allowed to settle; the sedimented microorganisms were transferred to new medium with sulfate and sulfide additions. Aliquots were then transferred to culture tubes incubated at their temperature optima (HR, 12 °C; MV, 20 °C) (21, 39).

Incubation Experiments with ^{35}S-Label. To measure the sulfate reduction rate by labeling, resuspended enrichments were distributed in amounts of 1 mL in 5-mL tubes. Tubes were completely filled (headspace-free) with anoxic synthetic seawater medium that was saturated with unlabeled CH_4 (under a gas phase of 150 kPa). Tubes were sealed with elastic butyl rubber. Controls were prepared with N_2 instead of CH_4 or with sterilized (20 g formaldehyde L^{-1}) cultures. A solution of ^{35}S-Na_2SO_4 (Amersham) was injected into a 5-mL culture tube. The specific activity in the medium was 5.5×10^8 Bq mol^{-1} (total sulfate concentration, 28×10^{-3} mol L^{-1}, for rate determination was assumed to be constant throughout the experiment). After 4 d, sulfide was recovered by a standard chromium reduction distillation method using a zinc acetate trap followed by scintillation counting. To preserve the settled cultures, 4 mL supernatant culture medium were transferred anoxically to 20 mL zinc acetate solution (0.9 M) to stop the reaction and fix sulfide. Radiolabeled ^{35}S product (total reduced inorganic sulfur) was separated from the radiolabeled reactant ($^{35}SO_4^{2-}$) by reduction with Cr^{2+} and cold distillation (54). The radioactivity of both pools was quantified by scintillation counting (scintillation mixture; LumaSafe Plus; scintillation counter, 2900TR LSA; Packard).

^{35}S-sulfide for labeling experiments was freshly generated from ^{35}S-Na_2SO_4 by bacterial reduction. *Desulfovibrio vulgaris* (DSM 2119) was incubated in a 20-mL tube containing 10 mL anoxic freshwater medium (53), H_2 gas (with 20% CO_2; 150 kPa total pressure) as electron donor, and 5×10^{-3} mol L^{-1} Na_2SO_4 with an adjusted label activity of 1.25×10^{11} Bq mol^{-1}. After complete reduction of sulfate, the culture was mixed with anoxic H_3PO_4 (5 mL at 1 mol L^{-1}). A slow N_2 stream was passed through the solution and headspace, through anoxic citrate buffer (10 mL at 0.1 mol L^{-1}, pH 4), and finally, through anoxic solutions of $ZnCl_2$ (15 mL at 0.4 mol L^{-1}) to trap sulfide. The collected ZnS suspension (a total of 75 mL) was acidified with H_3PO_4 (60 mL at 1 mol L^{-1}) under an N_2 headspace in an anoxic 156-mL vial to release labeled sulfide. The preparation through a gas phase and citrate buffer avoided transfer of other sulfur species that may have been present as impurities in the *Desulfovibrio* culture.

Labeled H_2S gas in N_2 was withdrawn in portions of 0.2 mL (6–9 kBq), injected into the headspace of 16-mL incubation vials with 10 mL medium and culture suspension, and for 24 h, equilibrated with the aqueous phase. Then, methane (200 kPa) was injected, and samples were incubated on

a rotary shaker. After 0, 3, 6, 8, 11, 15, and 19 d, four culture tubes (replicates) were used for analysis; 8 mL culture medium (biomass was maintained) were transferred to an anoxic zinc acetate solution (0.25 mol L^{-1}; 6 mL per tube) to fix sulfide. Total ^{35}S was determined in 100-μL aliquots from the ZnS suspension. $^{35}SO_4^{2-}$ was determined after thorough removal of ZnS by centrifugation (15 min, 2,500 × *g*) and ultrafiltration (Anotop 25 membrane filter, 0.02-μm pores; Whatman). Removal of ZnS was verified in filtrate aliquots by acidification with HCl (7 mol L^{-1}; 0.5 mL per mL), purging with N_2, and scintillation counting.

To analyze possible formation of ^{35}S-thiosulfate from labeled sulfide, unlabeled thiosulfate (final concentration of 1 mmol L^{-1}) was added to filtrate aliquots. Sulfate and thiosulfate were separated by an ion chromatograph (Waters) equipped with an IC-Pak anion exchange column (50 × 4.6 mm) and conductivity detector. The eluent was isophthalic acid (1 mmol L^{-1}, pH 4.5) in 10% aqueous methanol (10%, vol/vol; flow rate = 1.0 mL min^{-1}). The separated fractions were checked for ^{35}S. However, ^{35}S-thiosulfate was not detectable. Resulting samples with ^{35}S-label were mixed with LumaSafe Plus (Lumac LSC) and analyzed by liquid scintillation counting (TR-2900; Caberra-Packard).

Incubation Experiments with ^{14}C-Label. Resuspended enrichments were prepared similar to the sulfate reduction labeling experiment (see above). Controls were prepared with N_2 instead of CH_4 or without sulfate or with sterilized (20 g formaldehyde L^{-1}) cultures. CH_4 oxidation and back flux were measured by injecting $^{14}CH_4$ (American Radiolabeled Chemicals) or ^{14}C-$NaHCO_3$ (Perkin-Elmer), respectively, from aqueous solutions with high specific activity. Final specific activities in the medium were 6.5×10^8 Bq mol^{-1} for CH_4 (total concentration = 1.5×10^{-3} mol L^{-1}) and 4.5×10^8 Bq mol^{-1} for inorganic carbon (total concentration = 30×10^{-3} mol L^{-1}). After 4 d of incubation, 4 mL culture medium were fixed by transfer to 6 mL NaOH (0.6 mol L^{-1}) in a sealed glass vial (20 mL). Total methane was determined using a 5890A gas chromatograph (Hewlett Packard) equipped with a stainless steel Porapak-Q column (183 m × 3.2 mm, 80/100 mesh; Agilent) and flame ionization detector. Radioactivity of carbonate or methane was determined after separating both fractions. Methane was stripped off with air, oxidized at 850 °C with CuO, and trapped in 2-phenylethylamine base solution. Through acidification, carbonate was transferred into gaseous phase and again trapped in 2-phenylethylamine (55). Trap solutions were mixed with Ultima Gold XR (Perkin-Elmer) and analyzed in a 2900TR LSA liquid scintillation counter (TR-2900; Canberra-Packard).

Additional Analyses. Sulfide was determined colorimetrically using the methylene blue formation reaction in a miniaturized assay (56).

Determination of Reverse Reaction Rate. In catabolic conversion of substrate product with reversibility, A ⇌ P, forward and back flux (in the Introduction) are f_+ and f_- (moles volume^{-1} time^{-1}). When product label, P*, is added, appearance of A* reveals the back flux. If the label is a radioisotope with noticeable decay, error in label quantification is avoided by measuring radioactivity in all samples at the same time after the experiment; the specific isotope decay rate is independent of the chemical composition. The infinitesimal concentration d[A*] formed during an infinitesimal time d*t* depends on f_+ and f_-, heavy isotope discrimination in each direction (α_-, α_+; ≥1), and the proportion of label in total product and substrate (brackets indicate concentrations) (Eq. **12**):

$$\mathrm{d}[\mathrm{A}^*] = f_- \,\mathrm{d}t \frac{1}{\alpha_-}\frac{[\mathrm{P}^*]}{[\mathrm{P}]} - f_+ \mathrm{d}t \frac{1}{\alpha_+}\frac{[\mathrm{A}^*]}{[\mathrm{A}]}. \qquad [12]$$

Treatment is simplified by assuming that α_-, $\alpha_+ \sim 1$ and that the label proportion in the reactant pool remains very low ([A*]/[A] << [P*]/[P]), and therefore, return by f_+ can be neglected. Eq. **12** then yields (Eq. **13**)

$$\mathrm{d}[\mathrm{A}^*] = f_- \,\mathrm{d}t \frac{[\mathrm{P}^*]}{[\mathrm{P}]}. \qquad [13]$$

P* is increasingly diluted by steadily forming unlabeled P (*SI Text*, *Calculation of the Reverse Reaction Rate* and Fig. S3). If an increase Δ[A*] is measured after a short enough incubation time, Δ*t*, during which [P*]/[P] remains essentially constant, Eq. **13** can be simplified and rearranged to (Eq. **14**)

$$f_- = \frac{\Delta[\mathrm{A}^*]}{\Delta t}\frac{[\mathrm{P}]}{[\mathrm{P}^*]_0} = \frac{\Delta[\mathrm{A}^*]}{\Delta t}\frac{[\mathrm{P}]_0 + [\mathrm{P}^*]_0}{[\mathrm{P}^*]_0}. \qquad [14]$$

$[P]_0$ is the initial product concentration, and $[P^*]_0$ is the initial label concentration. If $[P^*]_0 << [P]_0$, Eq. **14** is simplified to (Eq. **15**)

$$f_- = \frac{\Delta[\mathrm{A}^*]}{\Delta t}\frac{[\mathrm{P}]_0}{[\mathrm{P}^*]_0} \qquad [15]$$

Such treatment is similar to the common determination of substrate fluxes in habitats by labeling and measuring product label (57, 58). We applied Eq. **15** to evaluate ^{14}C back fluxes in the methane–bicarbonate system. Back flux of inorganic carbon during AOM was determined, and $^{14}CH_4$ recovered from ^{14}C-bicarbonate after 4 d of incubation (endpoint measurement), applying Eq. **15** with Δ[A*] = [$^{14}CH_4$], $[P]_0$ = 0.031 mol L^{-1}, and [P*] = [$H^{14}CO_3$] added (C_{inorg} calculated from added $NaHCO_3/CO_2$ buffer). A high concentration of C_{inorg} was initially added as $NaHCO_3$ (30 mmol L^{-1}; a common natural buffer for cultivation of AOM consortia and many other anaerobes). Based on the net AOM rate derived from methane-dependent sulfide formation, C_{inorg} increased during incubation from 30 (initial) to ≤30.4 mmol L^{-1}.

In contrast to the concentration of bicarbonate, the concentration of sulfide was low at the beginning (<0.5 mmol L^{-1}). This concentration is advisable for cultivation of anaerobes, because sulfide can be inhibitory. However, now dilution of product label during AOM was significant, and [P] in Eq. **13** is expressed as a function of time. Assuming that the net rate, *v*, of A → P is largely independent of [A] (zero-order behavior, which is common in many microbial batch incubations) and that cell growth is negligible during incubation, the experimental data follow a straight-line fit with the slope f_-/v when displayed according to (derivation in *SI Text*, *Calculation of the Reverse Reaction Rate*) (Eq. **16**)

$$\ln\frac{[\mathrm{P}^*]_0}{[\mathrm{P}^*]_0 - [\mathrm{A}^*]} = \frac{f_-}{v}\ln\frac{[\mathrm{P}]}{[\mathrm{P}]_0}. \qquad [16]$$

Assuming the aforementioned prerequisites (negligible isotope fractionation, concentration-independent rates, and label concentration in the sulfate pool remaining low), we applied Eq. **16** with $[P^*]_0$ = [$H_2{}^{35}S$] added and [A*] = [$^{35}SO_4^{2-}$], [P] = [S_{red}], and $[P]_0$ = [S_{red}]$_0$ (S_{red} is chemically quantified sulfide). It has to be noted that the label concentration in the sulfate pool increases to the end of the incubation experiment to a level where label flux from the sulfate pool to the sulfide pool may no longer be negligible; application of Eq. **16** would then result in underestimation of the back flux. Chemical isotope exchange of ^{35}S between sulfide and zerovalent sulfur (e.g., elemental S or polysulfide S) (59) would dilute the specific activity of the sulfide pool (i.e., the effect would be the same). However, the linear trends for the data plotted in Fig. 1*C* and Fig. S2*C* indicate that the effect of such a label flux to the end of the experiment is within the error of the determined back fluxes (Table S2).

ACKNOWLEDGMENTS. We thank G. Schüssler for help during isotope analyses, G. L. Arnold for critical editing, and R. K. Thauer for constructive comments. This work was supported by the Max Planck Gesellschaft, the Bundesministerium für Bildung und Forschung (BMBF), and the Deutsche Forschungsgemeinschaft (DFG; Leibniz Program; to A.B.). This work is contribution number GEOTECH-1686 of the Research and Development Programme GEOTECHNOLOGIEN (BMBF and DFG) and Project Methane in the Geo/Bio-System - Turnover, Metabolism and Microbes (Grants 03G0554A and 03G0608A from BMBF).

1. Haldane JBS (1930) *Enzymes* (Longmans, Green & Co., London).
2. Boyer PD (1959) Uses and limitations of measurements of rates of isotopic exchange and incorporation in catalyzed reactions. *Arch Biochem Biophys* 82:387–410.
3. Cornish-Bowden A (2004) *Fundamentals of Enzyme Kinetics* (Portland Press, London).
4. Bisswanger H (2008) *Enzyme Kinetics: Principles and Methods* (Wiley, New York).
5. Purich DL (2010) *Enzyme Kinetics: Catalysis & Control: A Reference of Theory and Best-Practice Methods* (Elsevier Science, Amsterdam).
6. Thauer RK, Jungermann K, Decker K (1977) Energy conservation in chemotrophic anaerobic bacteria. *Bacteriol Rev* 41:100–180.
7. Thauer RK, Morris JG (1984) Metabolism of chemotrophic anaerobes: Old views and new aspects. *The Microbe: Part II: Prokaryotes and Eukaryotes*, eds Kelly DP, Carr NG (Cambridge University Press, Cambridge, UK), pp 123–168.
8. Schink B (1997) Energetics of syntrophic cooperation in methanogenic degradation. *Microbiol Mol Biol Rev* 61:262–280.
9. Jackson BE, McInerney MJ (2002) Anaerobic microbial metabolism can proceed close to thermodynamic limits. *Nature* 415:454–456.
10. Deppenmeier U, Müller V (2008) Life close to the thermodynamic limit: How methanogenic archaea conserve energy. *Results Probl Cell Differ* 45:123–152.

11. Stams AJM, Plugge CM (2009) Electron transfer in syntrophic communities of anaerobic bacteria and archaea. *Nat Rev Microbiol* 7:568–577.
12. Zehnder AJB, Brock TD (1979) Methane formation and methane oxidation by methanogenic bacteria. *J Bacteriol* 137:420–432.
13. Harder J (1997) Anaerobic methane oxidation by bacteria employing ^{14}C-methane uncontaminated with ^{14}C-carbon monoxide. *Mar Geol* 137:13–23.
14. Moran JJ, House CH, Freeman KH, Ferry JG (2005) Trace methane oxidation studied in several Euryarchaeota under diverse conditions. *Archaea* 1:303–309.
15. Moran JJ, House CH, Thomas B, Freeman KH (2007) Products of trace methane oxidation during nonmethyltrophic growth by *Methanosarcina*. *J Geophys Res* 112, G02011.
16. Meulepas RJW, et al. (2010) Trace methane oxidation and the methane dependency of sulfate reduction in anaerobic granular sludge. *FEMS Microbiol Ecol* 72:261–271.
17. Scheller S, Goenrich M, Boecher R, Thauer RK, Jaun B (2010) The key nickel enzyme of methanogenesis catalyses the anaerobic oxidation of methane. *Nature* 465:606–608.
18. Trudinger PA, Chambers LA (1973) Reversibility of bacterial sulfate reduction and its relevance to isotope fractionation. *Geochim Cosmochim Acta* 37:1775–1778.
19. Schauder R, Eikmanns B, Thauer RK, Widdel F, Fuchs G (1986) Acetate oxidation to CO_2 in anaerobic bacteria via a novel pathway not involving reactions of the citric acid cycle. *Arch Microbiol* 145:162–172.
20. Spormann AM, Thauer RK (1989) Anaerobic acetate oxidation to CO_2 by *Desulfotomaculum acetoxidans*. Isotopic exchange between CO_2 and the carbonyl group of acetyl-CoA and topology of enzymes involved. *Arch Microbiol* 152:189–195.
21. Nauhaus K, Boetius A, Krüger M, Widdel F (2002) *In vitro* demonstration of anaerobic oxidation of methane coupled to sulphate reduction in sediment from a marine gas hydrate area. *Environ Microbiol* 4:296–305.
22. Knab NJ, Dale AW, Lettmann K, Fossing H, Jørgensen BB (2008) Thermodynamic and kinetic control on anaerobic oxidation of methane in marine sediments. *Geochim Cosmochim Acta* 72:3746–3757.
23. Alperin MJ, Hoehler TM (2009) Anaerobic methane oxidation by archaea/sulfate-reducing bacteria aggregates: 1. Thermodynamic and physical constraints. *Am J Sci* 309:869–957.
24. Reeburgh WS (2007) Oceanic methane biogeochemistry. *Chem Rev* 107:486–513.
25. Knittel K, Boetius A (2009) Anaerobic oxidation of methane: Progress with an unknown process. *Annu Rev Microbiol* 63:311–334.
26. Hinrichs K-U, Hayes JM, Sylva SP, Brewer PG, DeLong EF (1999) Methane-consuming archaebacteria in marine sediments. *Nature* 398:802–805.
27. Boetius A, et al. (2000) A marine microbial consortium apparently mediating anaerobic oxidation of methane. *Nature* 407:623–626.
28. Orphan VJ, House CH, Hinrichs K-U, McKeegan KD, DeLong EF (2002) Multiple archaeal groups mediate methane oxidation in anoxic cold seep sediments. *Proc Natl Acad Sci USA* 99:7663–7668.
29. Niemann H, et al. (2006) Novel microbial communities of the Haakon Mosby mud volcano and their role as a methane sink. *Nature* 443:854–858.
30. Schreiber L, Holler T, Knittel K, Meyerdierks A, Amann R (2010) Identification of the dominant sulfate-reducing bacterial partner of anaerobic methanotrophs of the ANME-2 clade. *Environ Microbiol* 12:2327–2340.
31. Hoehler TM, Alperin MJ, Albert DB, Martens CS (1994) Field and laboratory studies of methane oxidation in anoxic marine sediment: Evidence for a methanogenic-sulfate reducer consortium. *Global Biogeochem Cycles* 8:451–463.
32. Treude T, et al. (2007) Consumption of methane and CO_2 by methanotrophic microbial mats from gas seeps of the anoxic Black Sea. *Appl Environ Microbiol* 73: 2271–2283.
33. Orcutt B, Samarkin V, Boetius A, Joye SB (2008) On the relationship between methane production and oxidation by anaerobic methanotrophic communities from cold seeps of the Gulf of Mexico. *Environ Microbiol* 10:1108–1117.
34. Sørensen KB, Finster K, Ramsing NB (2001) Thermodynamic and kinetic requirements in anaerobic methane oxidizing consortia exclude hydrogen, acetate, and methanol as possible electron shuttles. *Microb Ecol* 42:1–10.
35. Moran JJ, et al. (2008) Methyl sulfides as intermediates in the anaerobic oxidation of methane. *Environ Microbiol* 10:162–173.
36. Orcutt B, Meile C (2008) Constraints on mechanisms and rates of anaerobic oxidation of methane by microbial consortia: Process-based modeling of ANME-2 archaea and sulfate reducing bacteria interactions. *Biogeosciences* 5:1587–1599.
37. Meulepas RJW, Jagersma CG, Khadem AF, Stams AJM, Lens PNL (2010) Effect of methanogenic substrates on anaerobic oxidation of methane and sulfate reduction by an anaerobic methanotrophic enrichment. *Appl Microbiol Biotechnol* 87: 1499–1506.
38. Nauhaus K, Albrecht M, Elvert M, Boetius A, Widdel F (2007) *In vitro* cell growth of marine archaeal-bacterial consortia during anaerobic oxidation of methane with sulfate. *Environ Microbiol* 9:187–196.
39. Holler T, et al. (2009) Substantial $^{13}C/^{12}C$ and D/H fractionation during anaerobic oxidation of methane by marine consortia enriched *in vitro*. *Environ Microbiol Rep* 1: 370–376.
40. Cleland WW (1963) The kinetics of enzyme-catalyzed reactions with two or more substrates or products. I. Nomenclature and rate equations. *Biochim Biophys Acta* 67: 104–137.
41. Zehnder AJB, Brock TD (1980) Anaerobic methane oxidation: Occurrence and ecology. *Appl Environ Microbiol* 39:194–204.
42. Moore JW, Pearson RG (1981) *Kinetics and Mechanism* (Wiley, New York), 3rd Ed.
43. Rees CE (1973) A steady-state model for sulphur isotope fractionation in bacterial reduction processes. *Geochim Cosmochim Acta* 37:1141–1162.
44. Canfield DE (2001) Biogeochemistry of sulfur isotopes. *Rev Mineral Geochem* 43: 607–636.
45. Valentine DL, Chidthaisong A, Rice A, Reeburgh WS, Tyler SC (2004) Carbon and hydrogen isotope fractionation by moderately thermophilic methanogens. *Geochim Cosmochim Acta* 68:1571–1590.
46. Brunner B, Bernasconi SM (2005) A revised isotope fractionation model for dissimilatory sulfate reduction in sulfate reducing bacteria. *Geochim Cosmochim Acta* 69:4759–4771.
47. Penning H, Plugge CM, Galand PE, Conrad R (2005) Variation of carbon isotope fractionation in hydrogenotrophic methanogenic microbial cultures and environmental samples at different energy status. *Glob Change Biol* 11:2103–2113.
48. Johnston DT, Farquhar J, Canfield DE (2007) Sulfur isotope insights into microbial sulfate reduction: When microbes meet models. *Geochim Cosmochim Acta* 71: 3929–3947.
49. Farquhar J, Canfield DE, Masterson A, Bao H, Johnston DT (2008) Sulfur and oxygen isotope study of sulfate reduction in experiments with natural populations from Fællestrand, Denmark. *Geochim Cosmochim Acta* 72:2805–2821.
50. Eckert T, Brunner B, Edwards EA, Wortmann UG (2011) Microbially mediated re-oxidation of sulfide during dissimilatory sulfate reduction by *Desulfobacter latus*. *Geochim Cosmochim Acta* 75:3469–3485.
51. Tarpgaard IH, Røy H, Jørgensen BB (2011) Concurrent low- and high-affinity sulfate reduction kinetics in marine sediment. *Geochim Cosmochim Acta* 75:2997–3010.
52. Sim MS, Bosak T, Ono S (2011) Large sulfur isotope fractionation does not require disproportionation. *Science* 333:74–77.
53. Widdel F, Bak F (1992) Gram-negative mesophilic sulfate-reducing bacteria. *The Prokaryotes*, eds Balows A, Trüper HG, Dworkin M, Harder W, Schleifer K-H (Springer, New York), pp 3352–3378.
54. Kallmeyer J, Ferdelman TG, Weber A, Fossing H, Jørgensen BB (2004) A cold chromium distillation procedure for radiolabeled sulfide applied to sulfate reduction measurements. *Limnol Oceanogr Methods* 2:171–180.
55. Treude T, Krüger M, Boetius A, Jørgensen BB (2005) Environmental control on anaerobic oxidation of methane in the gassy sediments of Eckernförde Bay (German Baltic). *Limnol Oceanogr* 50:1771–1786.
56. Aeckersberg F, Bak F, Widdel F (1991) Anaerobic oxidation of saturated hydrocarbons to CO_2 by a new type of sulfate-reducing bacterium. *Arch Microbiol* 156:5–14.
57. Sorokin YI (1962) Experimental investigation of bacterial sulfate reduction in the Black Sea using S^{35}. *Microbiology* 31:329–335.
58. Jørgensen BB (1978) A comparison of methods for the quantification of bacterial sulfate reduction in coastal marine sediments. 1. Measurement with radiotracer techniques. *Geomicrobiol J* 1:11–27.
59. Fossing H, Jørgensen BB (1990) Isotope exchange reaction with radiolabeled sulfur compounds in anoxic seawater. *Biogeochemistry* 9:223–245.